Acta Materialia 242 (2023) 118473

Contents lists available at ScienceDirect

Acta Materialia

journal homepage: www.elsevier.com/locate/actamat

Magnetic properties of $NdFe_{11}Ti$ and $YFe_{11}Ti$, from experiment and theory

Heike C. Herper[a,*], Konstantin P. Skokov[b], Semih Ener[b], Patrik Thunström[a], Léopold V.B. Diop[c], Oliver Gutfleisch[b], Olle Eriksson[a,d]

[a] Department of Physics and Astronomy, Uppsala University, Box 516, SE-75120, Uppsala, Sweden
[b] Functional Materials, Department of Material Science, Technische Universität Darmstadt, 64287 Darmstadt, Germany
[c] Université de Lorraine, CNRS, IJL, F-54000 Nancy, France
[d] School of Science and Technology, Örebro University, Örebro SE-701 82, Sweden

ARTICLE INFO

Article history:
Received 15 June 2022
Revised 10 October 2022
Accepted 21 October 2022
Available online 27 October 2022

Keywords:
Permanent magnets
Rare-earths
Anisotropy
Magnetism
DFT
DMFT

ABSTRACT

$NdFe_{11}Ti$ and $YFe_{11}Ti$ serve as prototypes for rare-earth (RE) lean or REfree magnets with the $ThMn_{12}$-type structure. Although $NdFe_{11}Ti$ has been studied for a long time the origin of its complex magnetism at low temperature is so far not well-understood. We present a comprehensive theoretical and experimental study of the magnetic properties of $NdFe_{11}Ti$ and RE-free $YFe_{11}Ti$ to elucidate the influence of the $4f$ electrons. The partially localized $4f$ electrons of Nd are the driving force behind the complex behavior of the magnetocrystalline anisotropy which changes from cone to uniaxial above 170 dK. The spontaneous magnetization and the five leading anisotropy constants were determined from high-quality single crystal samples over a wide temperature range using field dependencies of magnetization measured along the principle crystallographic directions. The experimental data are compared with density functional theory combined with a Hartree-Fock correction (+U) and an approximate dynamical mean-field theory.

1. Introduction

The increasing awareness of the need for environment friendly technologies and green energy applications has caused an increasing demand for new high performance permanent magnets with less or no rare-earth (RE) elements compared to the standard $Nd_2Fe_{14}B$-type magnets. This has brought the rare-earth-lean Fe-based 1:12 systems $REFe_{12-x}Z_x$ ($ThMn_{12}$-type structure) back into the focus[1–7]. Although some Fe has to be substituted by another transition metal like Z = V, Ti, Mo, and Co [8], to stabilize the tetragonal phase, the 1:12 phases have a much better Fe to RE ratio than commercial $Nd_2Fe_{14}B$ magnets. The highest Fe to RE ratio can usually be achieved using Ti as substituent because only 1 out of 12 Fe ions must be replaced. Recently, we have shown that this also works for V if the RE element is Sm[3]. Large efforts are made to improve the magnetic properties of different 1:12 phases, e.g. by alloying with Co [2] to increase the Curie temperature or to improve the magnetocrystalline anisotropy energy (MAE) and T_C by adding light elements[6].

Though the phase stability is provided by the (usually) nonmagnetic dopants partially occupying the Fe sublattices, the magnetocrystalline anisotropy (MCA) is dictated to a large extend by the atom occupying the RE (2a) site[9].

At low temperatures some 1:12 compounds do not show the desired uniaxial MCA but possess a complex magnetic behavior connected to a spin-reorientation transition through a 1st or 2nd order phase transition [10]. For example, $NdFe_{11}Ti$ undergoes a spin reorientation transition somewhere between 178 K and 189 K [11,12] from a uniaxial to a cone anisotropy at lower temperatures. $TbFe_{11}Ti$, and $DyFe_{11}Ti$ [12] also undergo a spin-reorientation transition, whereas $YFe_{11}Ti$ and $SmFe_{11}Ti$ are uniaxial also at low temperatures[12]. In some cases the results are controversially discussed and various models have been applied to obtain a suitable description[10].

Since many applications take place at and above room temperature, the low-temperature properties, such as the cone MCA of $NdFe_{11}Ti$ are often not discussed. However, to gain a comprehensive insight in what drives the magnetism, a proper theoretical description should be able to capture the low-temperature properties of a material at the atomic scale. To this end, $NdFe_{11}Ti$ with its complex magnetic structure, and $YFe_{11}Ti$ as a rare-earth ($4f$ electron) free counterpart, serve as suitable benchmarks. To tackle the

* Corresponding author.
E-mail address: heike.herper@physics.uu.se (H.C. Herper).

https://doi.org/10.1016/j.actamat.2022.118473

theoretical approach needed to reproduce the experimental findings for the Nd-based system, we performed combined experimental and theoretical studies investigating the low-temperature magnetic properties of $NdFe_{11}Ti$ and $YFe_{11}Ti$ single crystals and performing electronic structure calculations in the framework of DFT. Even though the magnetism in $YFe_{11}Ti$ seems to be quite simple and well studied studied theoretically [2] and experimentally [13–15] there is some uncertainty or variation in the data. As for $NdFe_{11}Ti$ there exists quite some literature which focuses on $REFe_{12-x}M_x$. The reported results are diverse [2,5,12,16,17] and partially depend on preparation, material form (film, powder etc.), measurement method, e.g. Mössbauer or neutron diffraction[14,18]. In view of calculated properties the MCA values can largely differ in size and sign depending on the DFT method, e.g. basis set and exchange-correlation functional. [6,17] Körner et al.[2] obtained $K_1 = 4$ MJ/m^3 from LMTO (ASA) (Linear muffin tin orbital method within the atomic sphere approximation) calculations and computed crystal-field parameters while Harashima et al. find -0.8 MJ/m^3 from DFT [6]. Experimentally, 1.35 MJ/m^3 was reported at room temperature[19]. If the MCA is discussed in terms of crystal-field parameters, depending on the approximation and which crystal-field terms are taken into account, significant differences occur. For more details, see Guslienko *et al* and references therein[10]. However, modelling based on crystal field parameters often fails, because of a too large 6th order term, see Ref. [17] and references therein. An exception is the work by Kou et al. who fit the crystal field parameter to experimental results from susceptibility and magnetization measurements and achieved the correct behavior and predicted a cone angle of about 54°[12]. A similar angle has been predicted by Tajabor and co-workers from model calculations based on resistivity measurements on a polycrystalline sample[20].

Here, we compare DFT(+U) and DFT+DMFT (dynamical mean-field theory) calculations of $NdFe_{11}Ti$ and $YFe_{11}Ti$ to experimental values obtained from single crystals with a special focus on the low-temperature magnetism. We show that the magnetic properties of $NdFe_{11}Ti$ are crucially dependent on the description of the $4f$ electrons, i.e., the assumed degree of their localization. The paper is organized as follows: After a brief description of the theoretical, computational, and experimental methods in Section 2 the experimental results for the $NdFe_{11}Ti$ and $YFe_{11}Ti$ single crystals are presented in Section 3 since they are needed for the rating of the various theoretical approximations applied to derive the magnetic properties of the two systems. The following section (4 (a)) presents the basic theoretical results, i.e., the optimized geometry and the basic magnetic properties obtained from the DFT calculations for both systems. The main theoretical results for the MCA and related properties are presented in Section 4.2 followed by a summary and conclusion of the theoretical and experimental findings in Section 5.

2. Methods

2.1. Computational and theoretical aspects

Calculations use the primitive cell (13 atoms) in a tetragonal $ThMn_{12}$-type structure (space group 139), see Fig. 1. In such a structure the RE atoms occupy the 2a sites of the lattice while the Fe atoms are located on 8i, 8j, and 8f sites. Titanium dopants exclusively occupy 8i positions. The preference of the 8i site has been derived from x-ray diffraction by Yang et al[21]. Test calculations for Ti atoms on 8f and 8j sites confirmed the preference of Ti to occupy 8i sites in this geometry. Geometry optimizations are performed using the projected augmented wave method as implemented in the VASP code[22,23]. The generalized gradient approximation (GGA) in the formulation of Perdew, Burke, and Ernzerhof

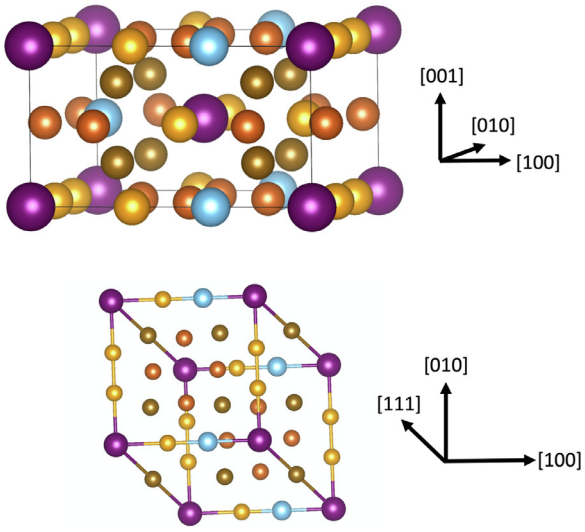

Fig. 1. Sketch of the unit cell (top) and primitive cell (bottom) of $REFe_{11}Ti$ with Ti sitting on an 8i site. Fe (Ti) atoms are marked by brown/yellow (blue) spheres. Large purple spheres denote Nd or Y atoms. In the primitive cell $x_1 = (a00)$, $x_2 = (0a0)$, and $x_3 = (0.5a, 0.5a, 0.5(c/a))$ with a being the lattice constant. (For interpretation of the references to colour in this figure legend, the reader is referred to the web version of this article.)

(PBE) [24] is used for the exchange correlation part of the energy functional. A k-point mesh of minimum 19^3 mesh points is used for these calculations. Systems are viewed as converged if forces are smaller than 10^{-3} eV/Å. The semi-core s- and p-states of all elements are included in the valence part whereas the $4f$ electrons of Nd are treated as core states during the structure optimization. The energy cut-off for the plane-wave expansion is 366.5 eV in both cases. Relaxations include only ionic relaxation, cell shape relaxation are neglected since the changes in the in[plane] lattice constants due to Ti on one of the 8i sites is small.

Full-potential linear muffin-tin orbital (FP-LMTO) calculations employing the RSPt code [25] are used to obtain the magnetic properties using the optimized geometries from the VASP calculations. The first set of calculations uses the same exchange correlation potential as for the geometry optimization for the sake of consistency. However, the magnetic properties are often better captured in a local spin density approximation (LSDA) description, additional investigations within the LSDA in the formulation of Vosko, Wilk and Nussair [26] are carried out using the geometry from the VASP/PBE calculations. A mesh of 24^3 k-points is adopted within the RSPt calculations and an expansion of the basis functions up to $l_{max} = 8$ is applied. MCA calculations in the framework of the magnetic force theorem (MFT) use an even denser k-point mesh with 35^3 points since the convergence of the eigenvalue sum is very sensitive to the k-point convergence.

While the investigations for $YFe_{11}Ti$ are straight forward, the ones for $NdFe_{11}Ti$ are more demanding due to the localized $4f$ electrons of Nd. Treating the localized electrons as valence electrons fails such that the magnetic properties are ill-described, see Section 4.1.2. Instead, a spin-polarized core approximation can be used. This has been successfully used for another related 1:12 system $SmFe_{12-x}V_x$[3]. However, we will show that this method is not really sufficient to capture the complex magnetic behavior of $NdFe_{11}Ti$. Therefore, additional calculations using DFT+U [27] are performed with U between 5.0 and 7.0 eV (LSDA+ U = 4.0–6.0 eV) whereby the J parameter was kept 1.1 eV in both cases (one test case is performed with a smaller J of 0.5 eV). Finally, to take also the dynamical correlation between the $4f$ electrons into account, we apply DMFT in the Hubbard-I-approximation (HIA)[28–30]. Tak-

ing $U = 5.6$ eV which was very close to the one with the optimal cone angle, see Section 4.2, i.e., we use LSDA and a Hubbard U of 5.6 eV (J = 1.1 eV) on the Nd $4f$ states. Unfortunately, the spin-polarized exchange-correlation functional produces an artificially large exchange splitting in $4f$ states in these calculations. Following the procedure described in Ref. [31] this can be cured and the calculations are made with a frozen local Hamiltonian.

2.2. Experimental method

A reliable comparison of the theoretical data to existing experimental literature data is problematic due to a large spread in values. Unambiguous determination of anisotropy constants requires high-quality single crystals. Here $NdFe_{11}Ti$ and $YFe_{11}Ti$ single crystals were grown by the reactive flux method using excess Nd and Y as a flux [32,33]. The first stage consisted in preparing the alloy of composition $Nd_2Fe_{11}Ti$ and $Y_2Fe_{11}Ti$ by melting high-purity constituting metals in an induction furnace under a purified atmosphere of argon in zirconia crucible. The so-obtained ingot was placed in new zirconia crucible, sealed in an evacuated quartz tube and annealed in a resistive furnace as follows: it was heated up to 1623 K at a rate of 300 K/h and kept at this temperature for 5 min in order to melt $Nd_2Fe_{11}Ti$ and $Y_2Fe_{11}Ti$ ingots. The temperature was reduced down to 1483 K at a rate of 300 K/h. Then, it was slowly cooled down to 1453 K during 13 days, kept there for 15 days, and finally quenched in water. This mode is favorable for growth of large crystalline grains. The ingot was broken up and several 1-mm-large grains were extracted. The strained surface layer of the grains was etched off electrolytically in phosphoric acid. The final composition was determined from energy-dispersive x-ray microanalysis and found to correspond to the desired stoichiometry $NdFe_{11}Ti$ and $YFe_{11}Ti$ respectively. The single-crystallinity control and orientation of the grains were performed by means of backscattering Laue x-ray diffraction. Magnetization curves were measured on oriented crystals in steady magnetic fields up to 14 T at various fixed temperatures ranging from 2 to 600 K using a Physical Property Measurement System (PPMS14 of Quantum Design).

3. Magnetic properties of $YFe_{11}Ti$ and $NdFe_{11}Ti$ single crystals

The magnetization curves for the $YFe_{11}Ti$ single crystal measured along the [100] and [001] crystallographic directions are displayed in Fig. 2(a). The demagnetization field was subtracted from the data using the known demagnetization factor of the sample. The $YFe_{11}Ti$ compound has uniaxial magnetic anisotropy in the whole temperature interval, i.e., the magnetic moments of Fe are parallel to the c axis and at 5 K the spontaneous magnetization of the $YFe_{11}Ti$ single crystal is 148.5 Am^2kg^{-1} that yields a magnetic moment of 1.82 μ_B per Fe atom (19.97 μ_B/f.u.). The initial increase of the magnetization in the hard direction [100] is linear and this linear growth is associated with magnetization rotation towards the field, continues practically to saturation. The linearity implies that fourth- and higher order anisotropy constants are negligible. At 5 K the anisotropy field is $\mu_0 H_a = 4.12$ T that corresponds to a magnetic anisotropy energy of 2.07 MJ/m^3. There is no significant difference between the magnetization curves measured along [100] and [110] directions, which means that the anisotropy in the basal plane can be neglected. The Sucksmith-Thompson technique is quite useful for evaluation of first two anisotropy constants K_1 and K_2 and this approach is traditionally applied for materials with uniaxial magnetic anisotropy [34,35]. The insert in Fig. 2(a) shows the temperature dependence of first anisotropy constant K_1 for $YFe_{11}Ti$ obtained by Sucksmith-Thompson technique in temperature range from 5 to 500 K. The second anisotropy constant does not exceed 2% of K_1 and is not presented in Fig. 2(a).

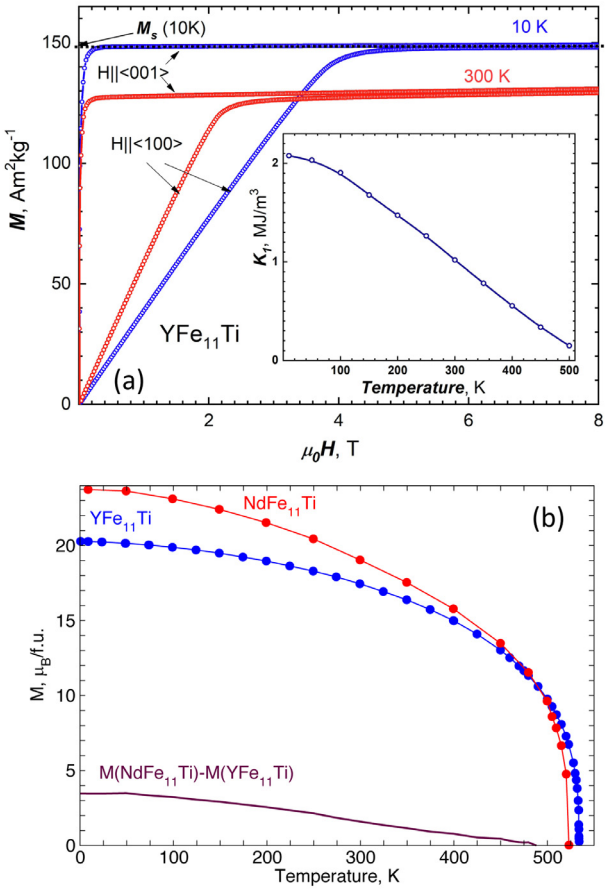

Fig. 2. (a) Magnetization curves measured along [100] and [001] crystallographic directions for $YFe_{11}Ti$ single crystal at 10 K and 300 K. (b) Spontaneous magnetization M_s of $YFe_{11}Ti$ and $NdFe_{11}Ti$ single crystals and magnetization of Nd-sublattice extracted using these data.

The spontaneous magnetization M_s of $YFe_{11}Ti$ was determined as the ordinate of the crossing point of the linearly extrapolated of the easy axis $M(H)$[001] curve to zero field (as shown on the 10 K curve in Fig. 2(a)). Near the Curie temperature the magnetization curve becomes essentially nonlinear and this simple way of determining M_s is no longer applicable. Therefore, at $T > 400$ K, M_s was deduced from the Belov Arrott graphs and Kuzmin plot, as described in detail elsewhere [36,37]. The spontaneous magnetization M_s for $NdFe_{11}Ti$ was measured on loose single crystal since at temperatures below 250 K the anisotropy of this compound changes from uniaxial to easy-cone type. M_s for both studied single crystals are plotted against temperature in Fig. 2(b). The Curie temperature of $YFe_{11}Ti$ is $T_C = 534$ K while for $NdFe_{11}Ti$ T_C is 523 K, and both T_C values are rather consistent with previously published data [13,38].

In order to estimate an effective magnetic moment for Nd, we subtract $M_s(T)$ of $YFe_{11}Ti$ from $M_s(T)$ of $NdFe_{11}Ti$ (up to the crossing point of the $M(Y)$ curves) as depicted in Fig. 2(b). At 5 K the difference between the two spontaneous magnetization values amounts to $M_s^{Nd}(T = 5K) = 3.47\mu_B$. This corresponds almost to the Nd moment obtained for the trivalent Nd ion in $Nd_2Fe_{14}B$ single crystal (3.27 μ_B) [39]. It should be noted that this effective moment of Nd $M_s^{Nd}(T)$ includes possible modulations of the magnetic moments of the Fe sublattices and the assumption that no contribution arises from the Y ion. In general, the Fe moment can vary in different $RFe_{11}Ti$ compounds due to changes in band structure caused by lanthanide contraction, shifting of Fermi level etc. All these factors can lead to some mismatch between $M_s^{Nd}(T)$ and the moment projected locally on Nd.

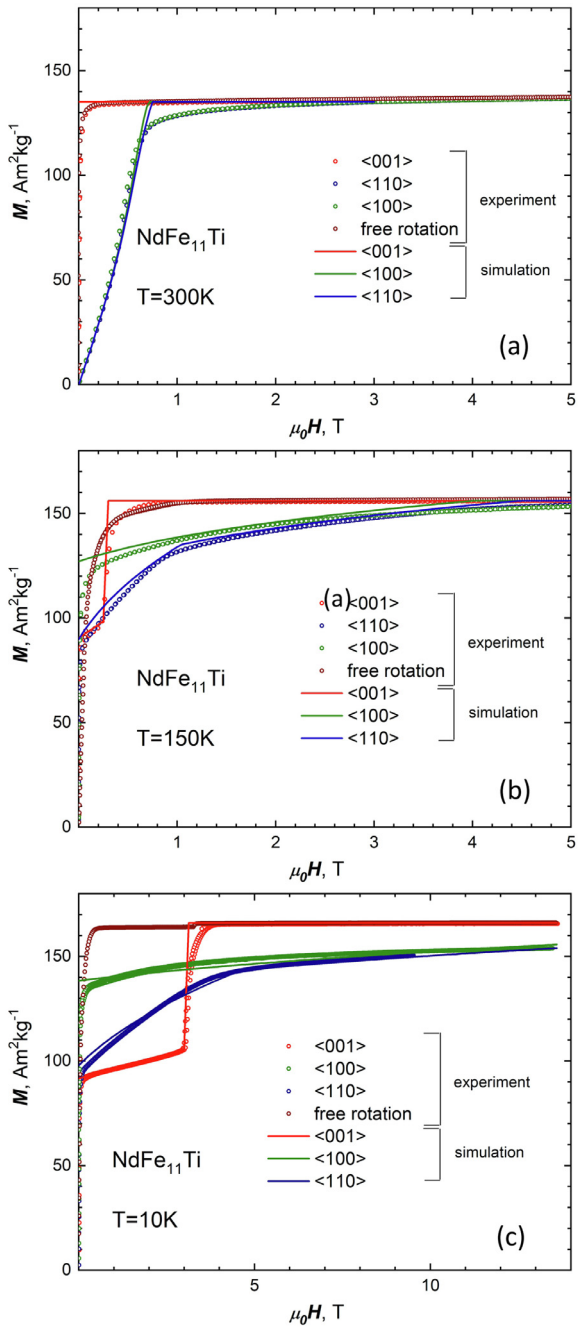

Fig. 3. Magnetization curves of $NdFe_{11}Ti$ single crystal measured along 3 principal crystallographic directions [100], [110] and [001] and the $M(H)$ of loose single crystal measured at $T = 300$ K (a), 150 K (b), and 10 K(c).

Fig. 3 shows the magnetization curves of $NdFe_{11}Ti$ single crystal measured along the three principal crystallographic directions [100], [110] and [001] and the fourth $M(H)$ dependence was measured on an unfixed sample (freely rotating) to always keep the orientation of the sample's easy axis along the direction of the external magnetic field. It can be seen that at 300 K the single crystal has uniaxial magnetic anisotropy with the anisotropy field $H_a = 0.8$ T (Fig. 3(a)). Upon decreasing temperature, a spin reorientation transition occurs at 170 K and at 150 K (Fig. 3(b)) $NdFe_{11}Ti$ exhibits easy-cone anisotropy. The jump in magnetization observed at the field of 0.3 T along [001] axis implies the existence of additional metastable minima of anisotropy energy along c-axis [40,41]. Fig. 3(c) shows the magnetization curves measured at 10 K. It is clear that at this temperature none of the principal crystallographic axes is the easy magnetization direction, which confirms that at low temperature the anisotropy type is of easy-cone. At the same time, there is a very pronounced abrupt rise of magnetization on the [001] curve around $\mu_0 H = 3$ T that is an evidence of complex character of magnetocrystalline anisotropy, which combines an easy-cone anisotropy with local metastable minima along the [001] direction. In this case, for unequivocal determination of anisotropy energy, together with K_1 and K_2 a higher-order anisotropy constants should be used. [40,42]

In order to determine the five leading anisotropy constants for $NdFe_{11}Ti$ single crystal, we used an approximation of experimental magnetization curves measured the three principal crystallographic directions by the simulated dependencies $M_{calc}(H)$ obtained in the framework of the Néel phase theory [43–46]. This method considers two magnetization processes: (i) the displacement of domain walls corresponding to the change in the volumes of magnetic domains with different orientation of magnetization, and (ii) the rotation of M_s in different types of magnetic domains toward the direction of the external field. The total energy of a crystal is represented by the energy of magnetocrystalline anisotropy, the Zeeman energy in the external field, and the energy of the demagnetizing field. The anisotropy energy up to 6th order can be written as:

$$E_A = K_1 \sin^2\phi + K_2 \sin^4\phi + K_2' \sin^4\phi \cos 4\theta + K_3 \sin^6\phi + + K_3' \sin^6\phi \cos 4\theta \quad (1)$$

where ϕ and θ are polar and azimuthal angles and K_i $(i = 1, 2, 3)$ and K_i' $(i = 2, 3)$ are the anisotropy constants. This technique allows to calculate the magnetization curves $M_{calc}(H)$ by using spontaneous magnetization M_s and anisotropy constants as input parameters. The set of anisotropy values, which provides the best fit, are considered to be the anisotropy constants obtained by this technique. In Fig. 3(a-c) calculated $M_{calc}(H)$ are shown as lines. One can see a good agreement of these simulated dependencies with our experimental data.

The temperature dependencies of first five anisotropy constants in the temperature range from 10 K to 300 K are shown in Fig. 4(a) and for temperature ranging between 200 K and 400 K the constants are depicted in Fig. 4(b). It can be seen that at temperatures above 300 K the anisotropy constant K_1 prevails, therefore, the $NdFe_{11}Ti$ has a clearly pronounced uniaxial magnetic anisotropy. In contrast to that, below 200 K the negative K_2 and positive K_3 overlap with other anisotropy constants, thence $NdFe_{11}Ti$ exhibits non-uniaxial complex magnetic anisotropy. The competition between K_2 and K_3 at low-temperatures results in coexistence of easy-cone anisotropy type with metastable uniaxial anisotropy, and this metastable minimum of anisotropy energy is responsible for pronounced jump in the magnetization when a magnetic field is applied along the c axis. Knowing the anisotropy constants allows us to find $E_a(\phi, \theta)$ for any possible combination of ϕ and θ. Fig. 4(c) shows the temperature dependence of the magnetocrystalline anisotropy energy $E_a(\phi, \theta)$ calculated for three different crystallographic axes of the $NdFe_{11}Ti$ single crystal. The anisotropy energy $E_a(0°, 0°)$ along [001] is notoriously zero for all temperatures, while at $T = 10$ K, $E_a(90°, 0°)$ along [001] reaches 0.81 MJ/m^3 and $E_a(90°, 45°)$ along [001] direction is 1.79 MJ/m^3.

The anisotropy constants K_1, K_2, K_2', K_3, and K_3' allowed us to calculate angular dependencies of the anisotropy energy at several selected temperatures when the magnetization rotates in 110 plane ($E_a(\phi, 45°)$, Fig. 5(a)) or in 100 plane ($E_a(\phi, 0°)$, Fig. 5(b)). One can see that at 10 K and in zero magnetic field, the magnetization lies within (100) crystallographic plane and takes an angle of 56° with the c-axis. As the temperature rises, the depth of this minimum becomes shallow and above 170 K the minimum

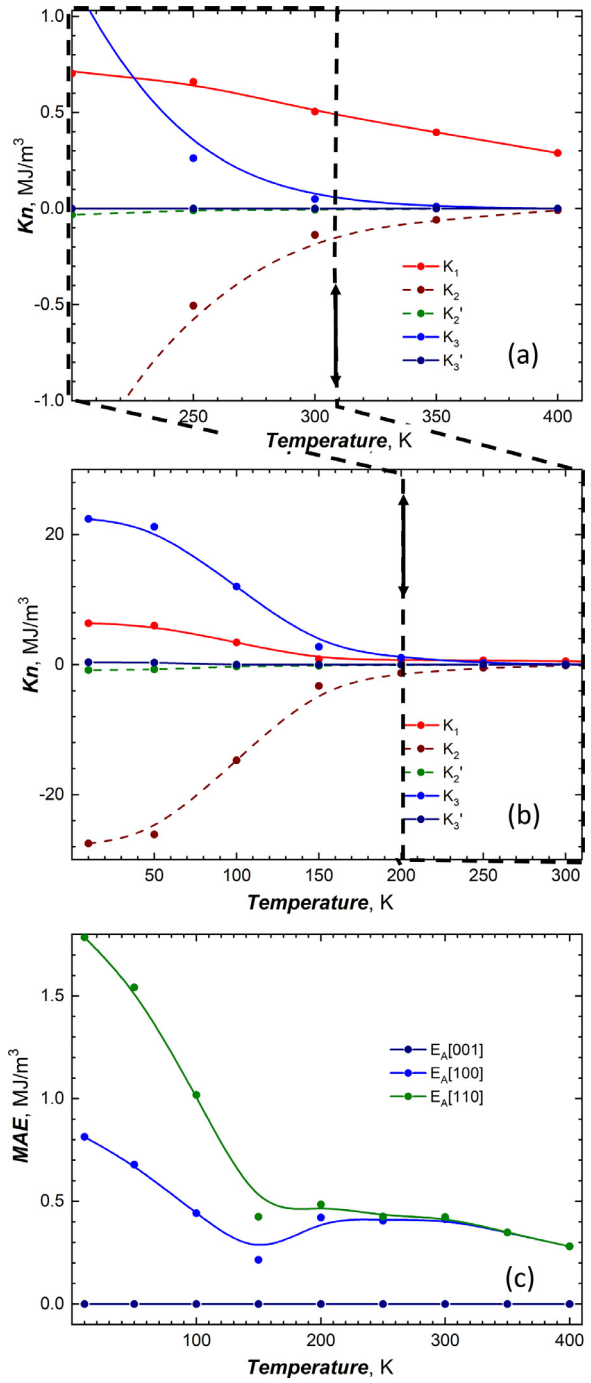

Fig. 4. (a,b) Temperature dependence of first five anisotropy constants K_1, K_2, K_2, K_3, and K_{3Prime} for $NdFe_{11}Ti$ single crystal whereby (b) shows the low-temperature region up to room temperature as indicated by the dashed box. (c) Temperature dependence of magnetic anisotropy energy (MAE) along 3 principal crystallographic directions.

of magnetocrystalline anisotropy energy (MAE) is located along the [001] axis, and the anisotropy changes to easy-axis type. It is worth noting that the angular position of the minima corresponding to easy cone anisotropy does not significantly shift with the temperature. This means that the transition at 170 K is of first-order type (the First-Order Magnetization Process [47–50]), where 2 magnetic phases with easy cone and easy axis anisotropy (or two different types of magnetic domains) co-exist during the transition. As an example of such a spin reorientation process one can see Ref. [50] which shows how the high-temperature uniaxial

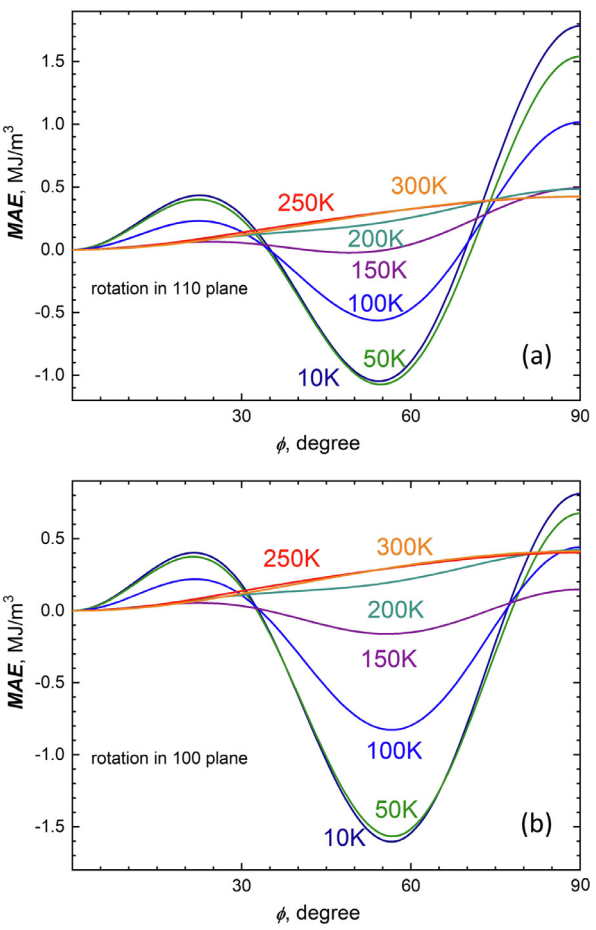

Fig. 5. Angular dependencies of the anisotropy energy at several selected temperatures when magnetization rotates (a) in (110) plane ($E_a(\phi, 45^\circ)$) and (b) in (100) plane $E_a(\phi, 0^\circ)$. (a,b) Temperature dependence of first five anisotropy constants K_1, K_2, K_2, K_3, and K_3' for $NdFe_{11}Ti$ single crystal and (c) Temperature dependence of magnetic anisotropy energy along three principal crystallographic directions.

magnetic phase of $Er_2Fe_{14}B$ turns in the low-temperature magnetic phase with easy-plane anisotropy.

4. Basic theoretical properties

4.1. Magnetization

The structural parameters obtained from the VASP calculations are in agreement with previous findings from theory and experiment, see Table 1. The average deviation between the measured lattice parameter or c/a ratio and our calculated data is between 0.5 and 1.5%, see Table 1. However, $YFe_{11}Ti$ is a good example of the well-known DFT dilemma and the choice of the exchange correlation functional. Though the geometry is well described in a DFT/PBE framework the magnetic properties are not. The magnetic trends of $YFe_{11}Ti$ are correctly reproduced but the magnitude of the magnetic properties is off. On the other hand LSDA wrongly predicts the structure and the preference of the Ti site [54]. In the following, different approximations have been applied to describe the magnetism in both systems and below we discuss their pros and cons.

4.1.1. $YFe_{11}Ti$

The calculated magnetic moments per formula unit and the magnetization values (Table 1) are within the expected range, but a more detailed look reveals a distinct dependence on the

Table 1
Structural and magnetic data for $REFe_{11}Ti$ (RE= Y, Nd). The lattice constant a and the ratio between the in-plane lattice constant and the tetragonal axis c/a are optimized using the VASP code [22,23], the magnetic data – magnetic moment (m) and Magnetization ($\mu_0 M$) – are taken from full-potential calculations within the RSPt code, for details see Section 2. The treatment of the Nd $4f$ electrons is given in the 1st column. Note in case of the spin-polarized core approximation the magnetization is too small due to the missing orbital moment.

	a	c/a	m_{2a}	m_{tot}	$\mu_0 M_s$
	(Å)		(μ_B)	(μ_B)	(T)
$YFe_{11}Ti$					
PBE	8.476	0.558	-0.73	22.01	1.51
LSDA[h]	8.476	0.558	-0.56	20.32	1.38
exp., here				19.97	
literature[a]	8.506	0.562		19.30	1.30
literature[b]	8.509	0.562			1.09
literature[c]	8.480	0.563		18.3	
literature[d]				18.4	
literature[e]				22.1	
$NdFe_{11}Ti$					
spinpol. core	8.578	0.550	–	25.19[i]	–
PBE+U=7.0	8.578	0.550	0.55	25.44	1.71
PBE+U=5.0	8.578	0.550	0.66	24.13	1.62
PBE	8.578	0.550	0.75	24.73	1.70
LSDA+U=5.3	8.578	0.550	2.45	23.39	1.57
LSDA+U=5.6	8.578	0.550	2.47	24.17	1.62
LSDA+DMFT	8.578	0.550	2.77	23.80	1.56
exp. here			3.47	23.43	
literature[f]	8.583	0.561		21.90	1.43
literature[g]	8.574	0.572		21.55	

[a] Ref. [13] at $T = 4.2$ K
[b] Ref. [51] magnetization at 300 K.
[c] Ref. [14] neutron diffraction, Mössbauer at 4.2 K.
[d] Ref. [15] liquid nitrogen temperature.
[e] Ref. [18] neutron diffraction
[f] Ref. [52] $T = 5$ K.
[g] Ref. [53] $T = 1.5$ K.
[h] 4f orbital moment from Hund's rules ($6\mu_B$)
[i] LSDA calculation with PBE optimized geometry, U =5.6 eV, J = 1.1 eV

exchange correlation potentials. For $YFe_{11}Ti$ experimental magnetic moments between 18.4 μ_B/f.u. [13,15] (Mössbauer) and 22.1 μ_B/f.u. [18] (neutron diffraction) have been reported whereas the value for a single crystal (this paper) amounts to 19.97 μ_B. The calculated magnetic moment obtained from RSPt with GGA (PBE) and spin-orbit coupling amounts to 22.04 μ_B/f.u. Even though PBE often describes the magnetic properties in RE systems correctly, e.g. in doped Ce_2Fe_{17} [55], it fails in others, such as for the undoped parent phase of the same system where PBE does not capture the complex ground state and overestimates the magnetic moment while LSDA agrees well with the experimental findings[56]. Therefore, we recalculated the magnetic properties using LSDA [26] keeping the geometry from the previous PBE calculations (analogous to what was done in Ref. [1]). Within the LSDA approximation the magnetic moment per formula unit decreases to about 20.3 μ_B/f.u. which is closer to the majority of the experimental findings.

Inspection of the site-projected moments reveals that the functional dependent shrinkage of the moment is a global effect, i.e., moments for all atoms decrease to a certain extend, with no preference of a single sublattice. Employing the PBE optimized structure means the lattice parameters used here are not at the equilibrium values for the LSDA calculations, i.e., the system experiences some stress since LSDA tends to have lower equilibrium volumes. The dilemma between structure and geometry impacts also the MAE which also depends on the volume, see Section 4.2.1. However, using the volumes from GGA and the magnetic moments from an LSDA approximation provides an excellent agreement with the experimental data obtained for the $YFe_{11}Ti$ single crystal. It should be noted that a final assessment whether LSDA or GGA/PBE is favorable would have been difficult from the magnetic moments and magnetization values from literature, because the difference between LSDA and GGA is about the same as between Mössbauer [38] and Neutron diffraction measurements[18].

4.1.2. $NdFe_{11}Ti$

In case of $NdFe_{11}Ti$ an additional layer of complexity enters the scene with the treatment of the $4f$ electrons of Nd which have a huge impact on the magnetic properties. Other than for $YFe_{11}Ti$, as discussed in Section 4.1.1, the level of the exchange correlation treatment has also an impact on the orientation of the magnetization axis, see Section 4.2.2.

Magnetic moments reported for $NdFe_{11}Ti$ range commonly between 20–22 μ_B per formula unit. [52,53,57,58] The measured value obtained for the single crystal in this work, 23.43 μ_B/f.u., lies a little higher compared to previous literature values. High-field free powder measurements of $NdFe_{11}Ti$ result in somewhat lower values, i.e., 18.4 μ_B have been reported solely for the transition metal part[57].

The total magnetic moment of $NdFe_{11}Ti$ from our calculations ranges between 23.39 and 25.44 μ_B/f.u., depending on approximation (see Table 1). Comparing the best theoretical results from DFT+U calculations ($U = 5.0$ eV for GGA and $U = 5.3$ eV for LSDA, $J = 1.1$ eV in both cases) to the magnetic moment obtained for the single crystal at 5 K (see Section 3) the deviation is less than 1% (3%) in LSDA (GGA). Treating the Nd $4f$ state as fully localized (i.e. as spin-polarized core electrons) we have direct access only to the spin contribution of the $4f$ moment, while the orbital moment is taken from Hund's rules. With this approximation the total moment is 25.19 μ_B whereby the spin contribution from the Nd ion ($4f, 5d, 6p$) is about -3.2 μ_B and the orbital moment is according to Hund's rules 6 μ_B. Assuming itinerant $4f$ electrons (PBE) the orbital moment can be directly calculated, and the total moment is then 24.73 μ_B, see Table 1. The total moments derived from the DFT+U calculations and even for plain DFT(GGA) are acceptably close to the measured values. Though the total moment is quite similar for different approximations, the Nd moment shows a strong dependence on the theoretical approach, i.e., the exchange correlation functional and corrections such as the U. In GGA-based calculations the projected total moment $m_s + m_l$ of Nd does not exceed 0.75 μ_B, see Table 1 and arises from an nearly cancellation of the $4f$ spin and orbital moment. In the LSDA+U approach the picture differs, since the total moment of the Nd ion is 2.30 μ_B while the bare $4f$ moment amounts to 2.45 μ_B. However, neither of these values are close to the effective Nd moment of 3.47 μ_B estimated for the single crystal just from the difference in magnetization between $YFe_{11}Ti$ and $NdFe_{11}Ti$ at 5 K (cf Section 3).

Knowing that DFT or even the DFT+U approach does not fully capture the physics of $4f$ electron systems we climbed up one step further on the ladder of theoretical descriptions using LSDA+DMFT. Encouraged by previous studies of Locht et al. for rare-earth elements [28] we applied the Hubbard I approximation to $NdFe_{11}Ti$, and found that the results for the total moment improved slightly. The total moment within the HIA approach reads 23.80 μ_B/f.u. (78 K) being in a very good agreement with our experimental value of 23.43 μ_B/f.u. (5 K). The projected Nd $4f$ moment is 2.77 μ_B (total moment of Nd including s, p, d orbitals is 2.62 μ_B) for magnetization axis along $\phi = 56^\circ, \theta = 0^\circ$ which is the easy cone orientation, see Section 4.2.2, is similar as in LSDA. Obviously the Hubbard I approximation improves the total moment but the moment projected on the Nd ion seems again to be lower than the effective value (see Table 1).

Nevertheless, if we do the same analysis as in experiment by comparing the two systems we find that the theoretical difference in total moments $m_{tot}^{NdFe_{11}Ti}(HIA) - m_{tot}^{YFe_{11}Ti}(LSDA) = 3.48$ μ_B is very

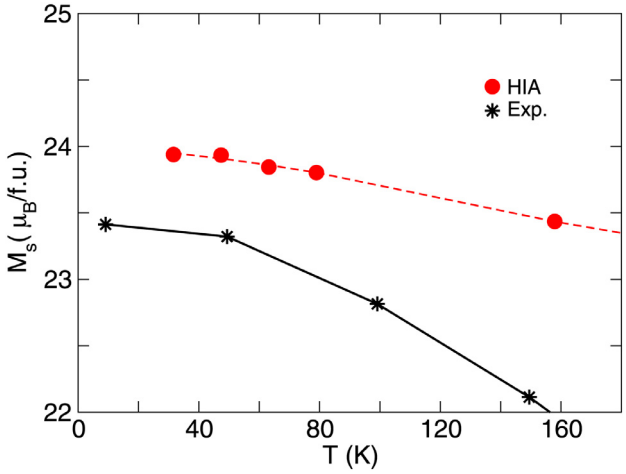

Fig. 6. Total magnetic moments for $NdFe_{11}Ti$ derived from the DMFT in Hubbard I approximation (red circles) compared to the experimental data for the single crystal (stars). Note, the HIA calculations have been performed with a fixed local Hamiltonian obtained for 78 K (Fermi smearing of 0.5 mRy) for details see Section 2. (For interpretation of the references to colour in this figure legend, the reader is referred to the web version of this article.)

close to the experimental value 3.47 μ_B. This implies, that the effective Nd moment cannot be fully attributed to Nd. A closer look at the calculated moments reveals that while moving from the Y- to the Nd-system the 3*d* transition metal moment changes by 0.83 μ_B and also Y possesses a finite moment of -0.58 μ_B. Taking these changes into account the calculated effective Nd moment becomes 3.23 μ_B with HIA and 2.82 μ_B in LSDA+U whereby the exact values depend on the choice of *U*. In conclusion of this section, we can state that the simple difference of the total magnetic moments does not reflect the Nd moment. The actual moment of Nd is smaller.

Since in the DMFT(HIA) approach the Fermi smearing translates directly to the bare electronic temperature we could even reproduce the temperature dependent increase of the magnetic moment of $NdFe_{11}Ti$ below 100 K, see Fig. 6. At higher temperatures the difference between the theoretical data and the measured values increases which is related to the onset of phonon contributions which are not included in the DMFT.

The figure of merit of a permanent magnet is the energy product $(BH)_{max}$ which is not accessible by DFT calculations in zero field. However, a rough estimation of $(BH)_{max}$ can be achieved. Ideally the hysteresis loop of a magnet would be square-shaped with no magnetization loss in the 2nd quadrant of the M(H) diagram. Thus $(BH)_{max}$ is simply given by $(\mu_0 M_s^2)/4$. [59] This can easily be estimated from ab initio calculations. In the present case $\mu_0 M_s$ is about 1.57 T for our system (LSDA, $U = 5.3$ eV, $J = 1.1$ eV) which corresponds to a $(BH)_{max}$ of about 490 kJ/m^3 (484 kJ/m^3 in HIA) being in the range of FePt or $Nd_2Fe_{14}B$[16].

4.2. Magnetocrystalline anisotropy

A key feature for the quality of permanent magnets is the magnetocrystalline anisotropy which can be determined from total energy differences or by employing the magnetic force theorem (MFT)[60]. The latter is often faster, but has a delicate *k*-mesh dependence. [61] In this work we use both total energy differences and MFT to compute the MCA. For both systems we studied the MCA depending on the angle between the tetragonal axis ([001]) and the magnetization studying the influence of various approximations on the size and sign of the MCA.

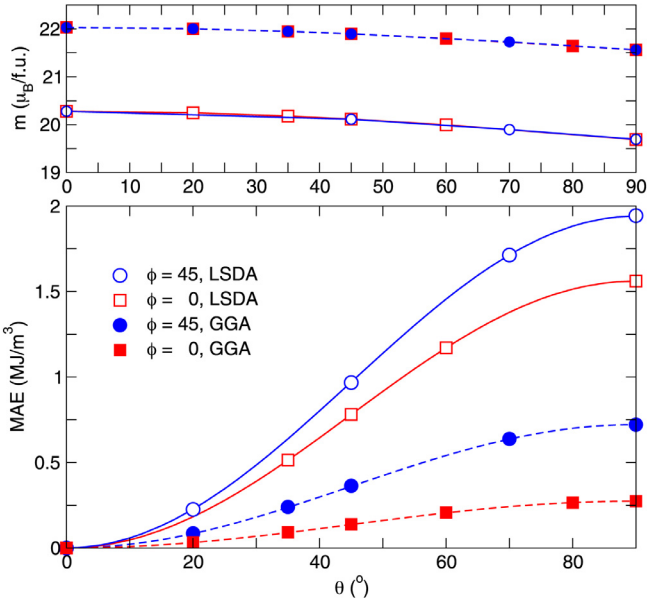

Fig. 7. Calculated magnetic moments per f.u. (a) and magnetocrystalline anisotropy (b) of $YFe_{11}Ti$ for varying angle θ. Squares (circles) denote changes from [001] to [100] ([110])orientation. Filled (open) symbols mark GGA (LSDA) results. The lines in (b) are fits according to Eq. 1 where only K_1 was taken into account. The black dashed-dotted lines denote the experimental values obtained within this study.

4.2.1. $YFe_{11}Ti$

To study the angular dependence of the MAE we have calculated the total energy for various angles (ϕ, θ) to simulate the movement of the magnetization axis from [001] to [100] and [110], respectively. In case of $YFe_{11}Ti$ the common assumption of the hard axis being in the basal plane along [110] is justified. The MAE from total energy differences $\Delta E = E_{[110]} - E_{[001]}$ amounts to 0.72 MJ/m^3 when the GGA(PBE) approximation is used and 1.94 MJ/m^3 in the LSDA description. The LSDA one is in very good agreement with the experimental findings for our $YFe_{11}Ti$ single crystal (2.07 MJ/m^3), cf Table 2 as well as with data reported by Qi et al. at helium temperature [38]. Though the absolute values are different, GGA and LSDA both correctly reveal that the system is uniaxial with easy axis along [001], see Fig. 7(b).

The angular dependence of the MCA is structure dependent and for tetragonal symmetry the anisotropy energy is given by Eq. 1 where ϕ is the polar angle between [001] and the magnetization direction and θ denotes the azimuth angle[16]. Here we consider only $\theta = 0°$ and 45°. $YFe_{11}Ti$ is known to have a uniaxial MCA such that the lowest order anisotropy constant, e.g. K_1, is sufficient to describe the MCA, for details regarding the anisotropy constants see Ref. [51] and references therein. We made some tests including K_2 but as expected the fitted values were in LSDA (GGA) 3 (almost 2) orders in magnitude smaller than K_1 and can safely be neglected.

All anisotropy data obtained from total energy differences $\Delta E = E_{[xyz]} - E_{[001]}$ and the fit to Eq. 1 are summarized in Table 2.

In case of $\Delta E = E_{[110]} - E_{[001]}$ we also calculated the MAE using the magnetic force theorem [60]. The differences between the two approaches appear to be very small and values differ at most 5%, see Table 2. The observed drop in the magnetization between easy and hard axis is about 0.03 T (0.5 μ_B/f.u.), see Fig. 7(a), independent from the exchange-correlation functional. Only the absolute values differ by about 2 μ_B.

The corresponding anisotropy field can be estimated from

$$H_a = \frac{2K_1}{\mu_0 M_s}. \quad (2)$$

Table 2
Calculated magnetocrystalline anisotropy for $YFe_{11}Ti$ from total energy differences (ΔE) and fitted to Eq. 1 for a first order fit with K_1 only. Data are provided for both LSDA and GGA formulations for the exchange-correlation potential. The $\Delta E/V$ value in brackets was obtained using the magnetic force theorem. κ denotes the hardness factor according to Eq. 3. The anisotropy field was derived from Eq. 2.

M direction	$\Delta E/V$ (MJ/m^3)		K_1 (MJ/m^3)		B_a(T)		κ	
	GGA	LSDA	GGA	LSDA	GGA	LSDA	GGA	LSDA
[110]	0.72 [0.65]	1.94	0.72	1.94	1.21	3.54	0.63	1.23
[100]	0.28	1.56	0.28	1.56	0.46	2.85	0.39	1.02
exp. this paper				2.07[d]				
exp. literature				1.89[a],1.91[b]		4.5[c]		

[a] Ref[51]., $T = 77$ K
[b] Ref. [13] $T = 4.2$ K original value 24 K/f.u. has been transformed to T;
[c] Ref. [53], $T = 1.5$ K, 45 kOe;
[d] 10 K, single crystal

The anisotropy field H_a is the upper limit for the coercivity field H_c, i.e., $H_a > H_c$ and is therefore an important factor for permanent magnets. However, in practise additional factors such as temperature dependence of K_1 and domain structure might come into play and the calculated values serve as ideal upper limit.

In case of LSDA we obtain $\mu_0 H_a = 3.5$ T, which is in the range of the values observed in experiment at low temperatures reaching from 3.4 T obtained from Mössbauer measurements [38] and 4.5 T [53] to 5.7 T [14] derived from neutron diffraction, see Table 2.

The underestimation of K_1 (see Table 2) and the too large magnetic moment obtained from GGA has direct impact on the theoretical anisotropy field, i.e., it leads to $\mu_0 H_a = 1.2$ T being 25% of the value reported from experiment.

Finally, the relation between the anisotropy constant and the magnetization determines the hardness of the magnet. The hardness factor is given by

$$\kappa = \sqrt{\frac{K_1}{\mu_0 M_s^2}} \tag{3}$$

where K_1 is the anisotropy constant and M_s denotes the saturation magnetization. κ values larger than 1 are considered to be the minimum requirement for hard permanent magnets. The hardness factor is $\kappa = 1.23$ (0.63) in LSDA (GGA).

In agreement with experiment an uniaxial MCA is found to be independent from the choice of the exchange correlation potential, although the values for GGA calculations deviate significantly in size. The calculated MCA values within the LSDA approach are on the other hand in very good quantitative agreement with our findings for the $YFe_{11}Ti$ single crystal at low temperatures and are comparable to the data reported in literature, see Table 2. The Ti atoms in our unit cell are in contrast to experiment not evenly distributed on the 8i sites, but concentrated on one specific site (Fig. 1) which breaks the symmetry between [100] and [010] orientation. Consequently, [110] will be an average of the MCA calculated from these two axis. Here, $E_{[010]} - E_{[001]}$ amounts to 2.31 MJ/m^3 (1.17 MJ/m^3) in LSDA (GGA) while $E_{[100]} - E_{[001]}$ gives only 1.56 MJ/m^3 (GGA = 0.28 MJ/m^3). Thus, it would be much harder to saturate the magnetization in [010], i.e., along the axis where the Ti sits, see Fig. 1.

What looked like a quite small difference in the last section (Section 4), i.e., the total magnetic moment differing by 2 μ_B between GGA and LSDA, multiplies for the MCA and related properties significantly. Thus, GGA underestimates the MCA by a factor of 2.6, see Table 2. To illustrate the relation between the structure and the magnetism additional fixed spin moment (FSM) calculations have been performed for $YFe_{11}Ti$. To do this the geometry was kept fixed to the one optimized within VASP/GGA and FSM calculations carried out in RSPt/GGA for total moments between

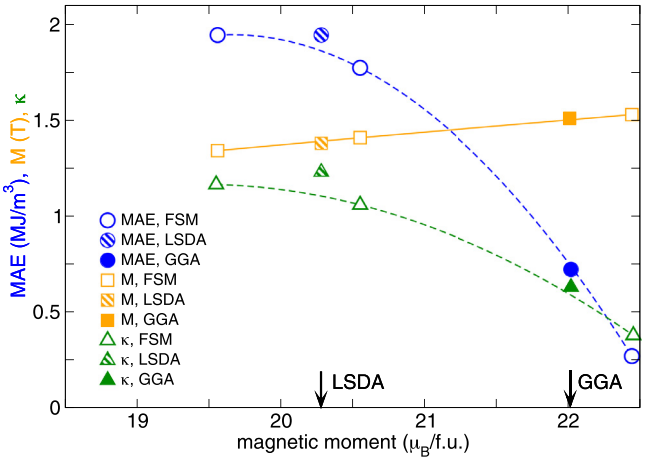

Fig. 8. Magnetocrystalline anisotropy (MAE), saturation magnetization (M), and hardness factor κ of $YFe_{11}Ti$ obtained from fixed spin moment (FSM) calculations using the GGA functional and the optimized lattice geometry. FSM data are marked by open symbols. For comparison the results for optimized structure and relaxed moments are also shown for GGA (filled symbols) and LSDA (hatched symbols). Arrows mark the total magnetic moment for LSDA and GGA calculations without FSM. Note the dashed lines are cubic spline fits through the FSM data.

19.5 and 22.5 μ_B/f.u. which corresponds to the range between GGA and LSDA or within experimental data, respectively. The magnetization for the LSDA and GGA calculation follow the linear behavior from the FSM magnetization curve. Thus the change in MCA and hardness between GGA and LSDA is reflected by just statically decreasing the total moment, i.e., decreasing the moment from 22.5 to 19.5 μ_B goes hand in hand with a nonlinear increase of the MAE and κ, see Fig. 8. However, the FSM calculations provide systematically smaller MCA values which also affect the hardness parameter. Fixing the total moment in GGA gives the right trend, i.e., magnetic properties improve with a moment reduction, but one would have to quench the moment beyond the LSDA value of 20.3 μ_B to achieve the same values, see Fig. 8.

Summarizing, in case of $YFe_{11}Ti$ DFT especially within the LSDA is capable to reproduce the magnetic properties reasonably well. This changes when moving to the sister compound $NdFe_{11}Ti$ due to the presence of the $4f$ electrons of Nd.

4.2.2. $NdFe_{11}Ti$

As mentioned above, $NdFe_{11}Ti$ is more complex from the viewpoint of magnetism exhibiting a cone MCA at low temperatures, cf Section 3. Assuming that due to its large spin-orbit coupling the main driving force of the MCA in RE-based phases is the $4f$ element, the description of the physics of the $4f$ states is essen-

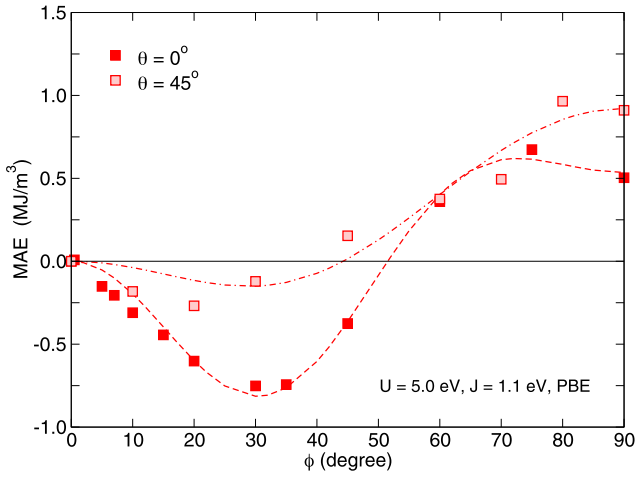

Fig. 9. Calculated magnetocrystalline anisotropy of $NdFe_{11}Ti$ for varying angle ϕ. Filled (hatched) symbols denote changes from [001] to [100] ([110]) orientation. The localization of the $4f$ electrons is described in GGA+U, with $U = 5.0$ eV and $J = 1.1$ eV. Lines denote fits of the calculated data to Eq. 1. All corresponding anisotropy constants are provided in the Supplement.

tial. Using the optimized structure described in Section 4 the magnetic characterization of the system has been made within a number of different approximations for the $4f$ electrons of Nd simulating different degrees of localization of the $4f$ states of Nd. Complete localization of these states can be described by using the spin-polarized core approximation in which the $4f$ electrons can carry a spin moment but do not overlap with the valences states. The contrary – fully itinerant $4f$ levels are described using plain DFT with the $4f$ states as valence states. Partial localization of the Nd $4f$ states can be expressed using the DFT+U approximation.

It turned out that the MCA is very sensitive to the choice of the localization level for the $4f$ states both in LSDA and GGA. Depending on the choice the calculated MCA is uniaxial or conic. If the $4f$ states of Nd would be fully localized with no hybridization between the $4f$ and the valence states the MCA appears to be uniaxial at low temperatures with an easy axis along [001]. The anisotropy constant K_1 (hard axis [110]) derived from Eq. 1 amounts to 0.554 MJ/m^3 ($K_2 = K_3 = 0$). However, the positive K_1 value, i.e., the uniaxial orientation of the MCA contradicts the experimental findings at low temperatures[11,12]. Reducing the level of localization by using a Hubbard U correction to the on-site Coulomb interaction improves the picture drastically. For U = 7 eV (J = 1.1 eV) the MCA of $NdFe_{11}Ti$ seems to still favor the [001] direction but in case of $\Phi = 0^\circ$ the angular dependence does not follow very well Eq. 1 so no definite determination is possible here. An unusual dip close to $\theta = 0^o$ appears (a detailed plot of the angular dependence can be found in the Supplement). The ratio between K_1 and K_2 points to a metastable anisotropy orientation[16]. Assuming an even lower degree of localization, i.e., using a smaller U value (here $U = 5$ eV, $J = 1.1$ eV) the rotation of the MCA away from the [001]-axis is observed, cf Fig. 9. If we ignore the cone and look only at the total energy differences between [110] and [001] direction of the magnetization, the MAE amounts to 0.95 MJ/m^3 which is smaller than the experimental value of 1.78 MJ/m^3 obtained for the single crystal (without taking into account the cone). For completeness we considered also the other extreme, itinerant $4f$ states, by handling the $4f$ electrons a valence electrons in a plain DFT/GGA approximation which resulted in a large uniaxial MCA with $K_1 = 9.7$ MJ/m^3. This is in contradiction to the experimental findings at low temperatures as well in sign and as in size.

From our calculations with $U = 5$ eV the angle between [110] and the easy magnetization axis is about $\phi = 26^\circ$, i.e., the systems shows a cone MCA. Fitting our data to Eq. 1 K_1 becomes -0.86 MJ/m^3 while K_2 turns out to be positive with $K_2 = 1.86$ MJ/m^3 such that the condition for a cone MCA $K_1 < 0$ and $K_2 > -K_1/2$ are fulfilled. The cone angle can then be derived from

$$\phi = \arcsin\left(\sqrt{\frac{|K_1|}{2K_2}}\right) \tag{4}$$

and reads 26°. If we move from [001] to [100] the anisotropy constants are different due to the choice of our cell in which the Ti atom sits on the [010] axis and is not homogeneously distributed over all 8i sites but the cone angle remains almost unchanged.

The angle agrees fairly well with the prediction of 35° (at 0 K) from crystal field theory by Hu et al. who extrapolated the value from the Dy counterpart [62], but admittedly differs from the experimentally determined values. A cone angle of 56° has been derived from our single crystal data and 54° were previously predicted from quadrupole-splitting[52]. Although our calculations reproduce the non-axial MCA they underestimate the angle, because the angles sensitively depend on the value of U, see supplement for details. However, we could demonstrate the influence of the description of the $4f$ electrons on the MCA. It should be noted that test calculations with MFT for the same k-point mesh resulted in smaller cone angles most probably due to a insufficient number of k-points. All calculated angles and anisotropy constants are provided in the supplemental material.

As shown in Section 4.2.1 for the sister compound $YFe_{11}Ti$ LSDA can improve the MCA results which is in agreement with earlier findings in literature. This motivated us to investigate the MCA of $NdFe_{11}Ti$ also within LSDA. Since the total energy calculations for DFT+U are quite costly we used here the MFT approximation which has led to very similar results in case of $YFe_{11}Ti$. A set of U values between 4 and 6 eV has been applied (J = 1.1 eV). The results are surprisingly different from the findings within the GGA. For U = 5 eV which has provided a cone MCA in the GGA case we observe a cone but with a smaller angle (21°), see Fig. 10. For smaller U values (4 eV) a uniaxial MCA is observed which corresponds to the trend observed in GGA. Increasing U goes hand in hand with a growing cone angle and with $U = 5.3$ eV and $J = 1.1$ eV the angle reaches 56° in agreement with the experimental data shown in Section 3. However, the anisotropy energy is tiny (0.24 MJ/m^3) and far smaller as the experimentally determined value 0.81 MJ/m^3 for our single crystal. Further increase of the Hubbard correction to $U = 6$ eV turns the MCA to the basal plane as can be seen from Fig. 10 (more details can be found in the Supplemental information). In this case K_1 is still negative but K_2 is no longer larger than $2|K_1|$. Neglecting the cone, the experimental MAE was found to be 1.79 MJ/m^3 ([110]). The closest in numbers is with 2.84 MJ/m^3 achieved for $U = 6$ eV, a U value for which no cone is observed. It should be mentioned that the cone was only observed when rotating from [001] to [100]. The anisotropy constants for rotation towards [110] point to uniaxial MCA. The reason might be that in the computation the Ti atoms are not evenly spread over all 8i sites. As discussed e.g. in Ref. [63] details of the chemical environment of the RE ion can have some influence on the magnetic properties of the system. However, an advantage of our description is, that it directly shows the effect of Ti on the magnetism when rotating along a direction with or without Ti. In GGA cone angles were observed for both rotations, even though the minimum for $\theta = 45^\circ$ was shallower. Therefore, it is very likely that the discrepancy between experiment and theory is not only due to the construction of the cell but at least partially also related to the exchange correlation functional.

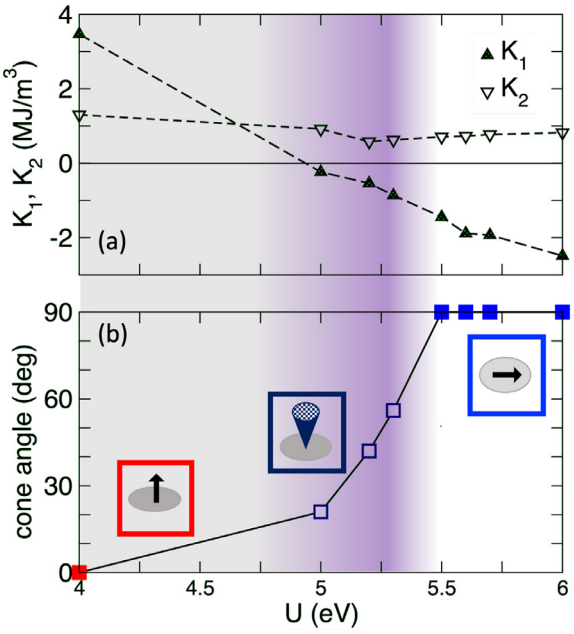

Fig. 10. (a) Calculated anisotropy constants K_1 and K_2 for $NdFe_{11}Ti$ depending on the size of the Hubbard U applied on the Nd $4f$ states. The corresponding J value was 1.1 eV in all calculations. (b) The resulting cone angle depending on U. The values were derived from Eq. 4.

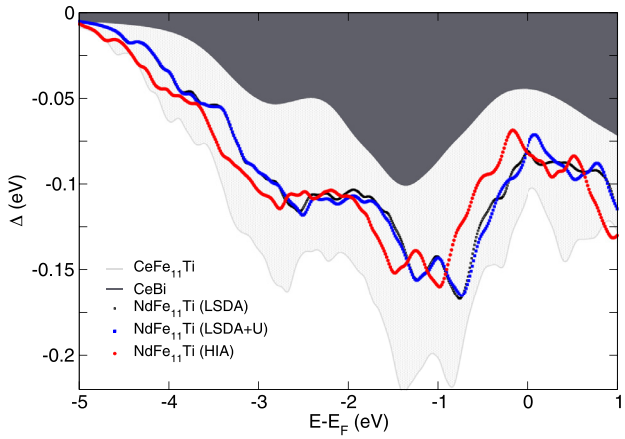

Fig. 11. Calculated hybridization function Δ of $NdFe_{11}Ti$ in comparison to $CeFe_{11}Ti$ and the strongly localized CeBi system (CeBi data are taken from Ref. [64] Δ is obtained from the Anderson impurity model and denotes the strength of interaction between the $4f$ impurity state and the surrounding valence electrons[64]. .

The above studies show that in contrast to other $REFe_{12}$ systems the Nd-phase is very sensitive to the description of the $4f$ electrons, i.e. their degree of localization. In case of $SmFe_{12-x}V_x$ the $4f$ electrons were fully localized and could be treated as core electrons[3]. For $CeFe_{11}Ti$ the change from spin-polarized core approximation to treating $4f$ electrons as valence electrons only influenced the magnitude of the MAE but the orientation remained uniaxial [4] while here magnitude and orientation depend on the approximation used to describe the localization of the $4f$ electrons of Nd. Our calculations suggest that the $4f$ electrons in $NdFe_{11}Ti$ are partially localized. To confirm this we looked at the hybridization function which can be viewed as a measure for the degree of localization of an electron. [64] To visualize the degree of localization in our case a comparison between the present system and two well-known Ce-based systems was made. We have chosen $CeFe_{11}Ti$ and the monopnictide CeBi for this purpose. Ce $4f$ electrons in $CeFe_{11}Ti$ are moderately localized and the magnetic properties can be reproduced in a DFT framework [4] while CeBi is a strongly localized system [30,64]. We plot the $4f$ hybridization function relative to the distance from the Fermi level of the three systems showing that $NdFe_{11}Ti$ lies indeed between the two reference cases. It should be noted that the level of theory, i.e. DFT, DFT+U, or HIA, has only very little impact on the hybridization function, for details we refer to Ref. [65]. From this it is understandable that the spin-polarized core approximation does not describe the magnetism correctly and it underpins our findings that the cone MCA could be described by a DFT+U approach with medium sized U of 5 eV simulating a not fully localized system.

Summarizing, to describe the low-temperature magnetic behavior of $NdFe_{11}Ti$ we have to go beyond DFT by at least adding a Hubbard U. Both extremes i.e. the spin-polarized core approximation and DFT with $4f$ states in the valence fail. In general, LSDA and GGA give a similar picture, i.e. a medium size U of about 5 eV is required to turn MCA in a cone while smaller values result in uniaxial MCA. In case of large U values or fully localized $4f$ states easy-plane or metastable solutions appear.

5. Summary and conclusion

Tetragonal RE-lean 1:12 phases bare a huge potential for future permanent magnets and predicting new suitable candidates from materials design seems a promising road to go. A prerequisite for successful predictions is mastering the description of the magnetism in these systems which boils down to an accurate description of the $4f$ electrons of the RE ions and the Fe sublattices. To identify a scheme which can be used for materials design on new 1:12 permanent magnets we performed a comprehensive experimental and theoretical study of $NdFe_{11}Ti$ as an example for a 1:12 phase magnet. We believe that our findings are not limited to the description of the example system but are also relevant for studies of related 1:12 phases with Nd, such as $RE_{1-x}Nd_xFe_{12-y}Ti_y$ which have not been synthesized and investigated to this day.

Though, the MCA of $REFe_{12}$ based phases has been part of numerous theoretical studies and different theoretical approaches have been used, the complex low-temperature behavior is less often addressed. Believing that the calculational methods should capture correctly low-temperature magnetic properties including the cone-type MCA of $NdFe_{11}Ti$ we were looking for a suitable theoretical approach. The aim of this extensive study was not only to describe the magnetism of $NdFe_{11}Ti$ but to find a method which allows us to predict the properties of new Nd-based 1:12 systems which have not been synthesized so far. Since the magnetism of RE compounds is largely determined by the behavior of the $4f$ electrons of the RE ions we needed a method which can handle the $4f$ electrons and their subtle correlation effects accurately.

A close look to the literature revealed a large spread in experimental results which would make it difficult to determine the *best* theoretical description. Therefore, we grew single crystals of the two materials to have clean samples to compare with. For the yttrium compound we achieved uniaxial MCA as expected with anisotropy energy being 2.07 MJ/m^3. The low-temperature measurements of the Nd-based sample showed a cone type MCA with an angle of 56° and anisotropy energies of 0.81 MJ/m^3 and 1.79 MJ/m^3 for [100] and [110], respectively.

In order to understand which theoretical description best reproduces the experimental findings, we studied the magnetic properties of $YFe_{11}Ti$ and $NdFe_{11}Ti$ depending on various theoretical approximations whereby the well-known Y compound served as test system. As partially reported in literature, for $YFe_{11}Ti$ the best agreement with experimental data is obtained from LSDA with the structure being optimized within the GGA. The dependence on the functional (LSDA, GGA) was studied alongside with different ap-

proximations for the $4f$ states of Nd (DFT, DFT+DMFT). The key point here is the handling of the $4f$ electrons and taking into account the localization effects properly. The influence of the theoretical approach used to describe the physics of the $4f$ states in Nd-based $REFe_{12}$ phases has been discussed on the example of $NdFe_{11}Ti$.

Our studies show that the $4f$ electrons in $NdFe_{11}Ti$ can not be treated as fully localized. Using a moderate Hubbard U correction ($U \approx 5$ eV (GGA)) on the Nd $4f$ states the cone MCA could be reproduced with an angle of about 30° between magnetization and [001] or [110] direction. In case of LSDA we were able to show that the cone angle can be adjusted by changing the U value and for U= 5.3 eV the experimental value was obtained. However, rotation from [001] to [110] did not lead to a cone type MCA most probably due to the construction of the cell. Large U values lead to easy-plane MCA in LSDA and metastable configurations in GGA, while the spin-polarized core approximation (GGA), which simulates full localization predicts a uniaxial MCA.

In addition to the MCA we compared the magnetic moments of the different calculations, however other than for the Y-compound the differences between LSDA and GGA were not so huge and partially covered by the use of U. However, using LSDA with U = 5.3 eV and $J = 1.1$ eV we could reproduce not only the MCA orientation but also the experimentally obtained moment of the Nd system (theory: 23.39 μ_B, experiment 23.43 μ_B).

Another frequently raised question concerns the size of the moment of the Nd ion in $NdFe_{11}Ti$. The experimental approach is very indirect e.g. the Nd moment is estimated from a comparison between $NdFe_{11}Ti$ and $YFe_{11}Ti$ total moments and based on the assumption that the transition metal moments stay unchanged. Ab initio methods allow a closer look at the system and the distribution of the magnetic moments. Thus, we could directly extract the magnetic moment projected on every ion and already in LSDA+U approximation we saw deviations from the experimental assumptions. Therefore, we performed a more accurate DFT+DMFT study. The total moment is almost unchanged in DFT+DMFT compared to DFT+U (HIA: 23.80 μ_B) i.e. the difference of the total moments of $NdFe_{11}Ti$ and $YFe_{11}Ti$ amounts to 3.48 μ_B in HIA. A detailed analysis of the projected moments revealed that the difference is not only due to the Nd moment. The actual Nd moment is smaller than the total change and amounts only to 2.62 μ_B in HIA. We observe that the transition metal moment also changes (about 0.83 μ_B) and the Y moment cannot be neglected. This is not completely unexpected and might be related to the change in the lattice structure and atomic distances.

Though the DMFT approach has been proven very accurate and successful, it is not parameter-free and computationally demanding. Aiming to find a theoretical set up which is transferable to other so far unexplored Nd 1:12 systems and can be used later e.g. also in a high throughput type study a DMFT approach is not practical and too dependent on the electronic details of the system under investigation. Further, a conversion of the energies to the level needed for the determination of the magnetocrystalline anisotropy would be very challenging.

Summarizing, the comparison of the results from the various calculations with the data obtained from the two single crystals confirmed for our benchmark system $YFe_{11}Ti$ the discussion in literature and LSDA is clearly favorable for the magnetic properties. In case of $NdFe_{11}Ti$ it is not so obvious since the description of the magnetic properties is more complex but overall a LSDA scheme is also here preferable though not in plain DFT as it is done in some publications but with a U at least. Going beyond a DFT+U approach leads to further improvement but might due to its complexity not be applicable for studies of new systems where experimental data are lacking. The DFT+U approach might be used at least if the changes composition are not too extensive and can be used for the search for new candidate phase for 1:12-based permanent magnets.

Declaration of Competing Interest

The authors declare that they have no known competing financial interests or personal relationships that could have appeared to influence the work reported in this paper.

Acknowledgement

HCH thanks Johan Jönsson for support and discussion around the DMFT calculations. We acknowledge funding from the HORIZON-2020 project NOVAMAG (EU 686056), the Swedish Strategic Research Foundation (SSF) (Grant EM16-0039), STandUPP, eSSENCE, The Swedish Energy Agency (STEM) as well as from Vetenskapsrdet (VR). KS and OG thank the Deutsche Forschungsgemeinschaft (DFG, German Research Foundation), Project ID No. 405553726-TRR 270. The computations were performed on resources provided by Swedish National Infrastructure for Computing (SNIC) at PDC and LIU.

Supplementary material

Supplementary material associated with this article can be found, in the online version, at doi:10.1016/j.actamat.2022.118473.

References

[1] L. Ke, D.D. Johnson, Intrinsic magnetic properties in $R(Fe_{1-x}Co_x)_{11}TiZ$ (R = Y and Ce; Z = H, C and N), Phys. Rev. B 94 (2016) 024423, doi:10.1103/PhysRevB.94.024423.

[2] W. Körner, G. Krugel, C. Elsässer, Theoretical screening of intermetallic $thmn_{12}$-type phases for new hard-magnetic compounds with low rare earth content, Sci. Rep. 6 (2016) 24686, doi:10.1038/srep24686.

[3] A. Schönhöbel, R. Madugundo, O.Y. Vekilova, O. Eriksson, H. Herper, J. Barandiaran, G. Hadjipanayis, Intrinsic magnetic properties of $SmFe_{12-x}V_x$ alloys with reduced v-concentration, J. Alloys Compd. 786 (2019) 969–974, doi:10.1016/j.jallcom.2019.01.332. http://www.sciencedirect.com/science/article/pii/S0925838819303585.

[4] R. Martinez-Casado, A. Dasmahapatr, M.F. Sgroi, C. Romero-Muñiz, H.C. Herper, O.Y. Vekilova, A.M. Ferrari, D. Pullini, J. Desmarais, L. Maschio, The $CeFe_{11}Ti$ permanent magnet: a closer look at the microstructure of the compound, J. Phys.: Cond. Matt. 31 (2019) 505505.

[5] H.I. Sözen, S. Ener, F. Maccari, K.P. Skokov, O. Gutfleisch, F. Körmann, J. Neugebauer, T. Hickel, Ab initio phase stabilities of ce-based hard magnetic materials and comparison with experimental phase diagrams, Phys. Rev. Materials 3 (2019) 084407, doi:10.1103/PhysRevMaterials.3.084407.

[6] Y. Harashima, K. Terakura, H. Kino, S. Ishibashi, T. Miyake, Nitrogen as the best interstitial dopant among X=B, C, N, O, and F for strong permanent magnet $NdFe_{11}TiX$: first-principles study, Phys. Rev. B 92 (2015) 184426, doi:10.1103/PhysRevB.92.184426.

[7] S. Ener, K.P. Skokov, D. Palanisamy, T. Devillers, J. Fischbacher, G.G. Eslava, F. Maccari, L. Schfer, L.V. Diop, I. Radulov, B. Gault, G. Hrkac, N.M. Dempsey, T. Schrefl, D. Raabe, O. Gutfleisch, Twins a weak link in the magnetic hardening of $ThMn_{12}$-type permanent magnets, Acta Mater. 214 (2021) 116968, doi:10.1016/j.actamat.2021.116968. https://www.sciencedirect.com/science/article/pii/S1359645421003487.

[8] T.S. Chin, W.C. Chang, H.C. Ku, C.C. Weng, H.T. Lee, M.P. Hung, Structure and magnetic properties of the $ThMn_{12}$ type NdFeM (M=Si/Al/B/transition metals) alloys, IEEE Trans. Magnet. 25 (1989) 3300.

[9] J. Coey, Perspective and prospects for rare earth permanent magnets, Engineering 6 (2) (2020) 119–131, doi:10.1016/j.eng.2018.11.034. https://www.sciencedirect.com/science/article/pii/S209580991830835X.

[10] K.Y. Guslienko, X.C. Krou, R. Grössinger, Magnetic anisotropy and spin-reorientation transion in $RFe_{11}11Ti$ (R = Nd, Tb, Dy, Er) rare-earth intermetallics, J. Magn. Magn. Mater. 150 (1995) 383.

[11] N.H. Luong, N. Thuy, J. Franse, Spin reorientation in $Nd_{1-x}Y_xFe_{11}Ti$, J. Magn. Magn. Mater. 104–107 (1992) 1301.

[12] X.C. Kou, T.S. Zhao, R. Grossinger, H. Kirchmayr, X. Li, F.R. deBroer, Magnetic phase transitions, magnetocrystalline anisotropy, and crystal-field interactions in the $RFe_{11}Ti$ series (where R=Y, Pr, Nd, Sm, Gd, Tb, Dy, Ho, Er, or Tm), Phys. Rev. B 47 (1993) 3231.

[13] I.S. Tereshina, V.S.R. P. Gaczyński, S.A. Nikitin, W. Suski, N.V. Tristan, T. Palewski, Magnetic anisotropy and mssbauer effect studies of YFe_{11}ti and $YFe_{11}TiH$, J. Phys.: Cond. Matt. 13 (2001) 8161.

[14] S. Obbade, D. Fruchart, M. Bououdina, S. Miraglia, J. Soubeyroux, O. Isnard, About hydrogen insertion in $ThMn_{12}$ type alloys, J. Alloys Compd. 253–254 (1997) 298–301, doi:10.1016/S0925-8388(96)02900-3. http://www.sciencedirect.com/science/article/pii/S0925838896029003.

[15] H. Suzuki, Metastable phase YFe_{12} fabricated by rapid quenching method, AIP Adv. 7 (2017) 056208.

[16] J.M.D. Coey, Magnetism and magnetic materials, Cambridge University Press, Cambridge, UK, 2010.

[17] C. Piquer, F. Grandjean, O. Isnard, G.J. Long, A phenomenological model for the rare-earth contribution to the magnetic anisotropy in $RFe_{11}Ti$ and $RFe_{11}TiH$, J. Phys.: Condens. Matter 18 (2006) 221.

[18] Y. chang Yang, H. Sun, L. shu Kong, J. lian Yang, Y. fan Ding, B. sheng Zhang, C. tang Ye, L. Jin, H. ming Zhou, Neutron diffraction study of $Y(Ti,Fe)_12$, J. Appl. Phys. 64 (1988) 5968, doi:10.1063/1.342165.

[19] M.Akayama, H. Fujii, K.Yamamoto, K.Tatami, Physical properties of nitrogenated $RFe_{11}ti$ intermetallic compounds (R=Ce, Pr and Nd) with $thmn_{12}$-type structure, J. Magn. Magn. Mater. 130 (1994) 99, doi:10.1016/0304-8853(94)90662-9.

[20] N. Tajabor, A. Amirabadizadeh, M. Alinejad, F. Pourarian, Anomalous behavior of electrical resistivity in $NdFe_{11}Ti$, phys. stat. sol. (c) 1 (2004) 1788, doi:10.1002/pssc.200304406.

[21] Y.C. Yand, X.D. Yang, L. Kong, Q. Pan, S.L. Ge, J.L. Yang, Y. Ding, B.S. Zhang, C.T. Ye, Neutron diffraction study of the nitride $YTiFe_{11}N_x$, Sol. State Commun. 78 (1991) 313.

[22] G. Kresse, J. Hafner, Ab initio molecular-dynamics simulation of the liquid-metal amorphous-semiconductor transition in germanium, Phys. Rev. B 49 (1994) 14251.

[23] G. Kresse, J. Furthmüller, Efficiency of *ab initio* total energy calculations for metals and semiconductors using a plane-wave basis set, Comp. Mater. Sci. 6 (1996) 15.

[24] J. Perdew, S. Burke, M. Ernzerhof, Generalized gradient approximation made simple, Phys. Rev. Lett. 77 (1996) 3865.

[25] J.M. Wills, M. Alouani, P. Andersson, A. Delin, O. Eriksson, O. Grechnyev, Full-Potential electronic structure method, Springer series in solid state science, volume 167, Springer, Berlin, Germany, 2010.

[26] S.H. Vosko, L. Wilk, M. Nusair, Accurate spin-dependent electron liquid correlation energies for local spin density calculations: a critical analysis, Can. J. Phys. 58 (1980) 1200.

[27] A.I. Liechtenstein, V.I. Anisimov, J. Zaanen, Density-functional theory and strong interactions: orbital ordering in mott-hubbard insulators, Phys. Rev. B 52 (1995) R5467.

[28] I.L.M. Locht, Y.O. Kvashnin, D.C.M. Rodrigues, M. Pereiro, A. Bergman, L. Bergqvist, A.I. Lichtenstein, M.I. Katsnelson, A. Delin, A.B. Klautau, B. Johansson, I. Di Marco, O. Eriksson, Standard model of the rare earths analyzed from the hubbard i approximation, Phys. Rev. B 94 (2016) 085137, doi:10.1103/PhysRevB.94.085137.

[29] P. Thunström, I. Di Marco, A. Grechnev, S. Lebègue, M.I. Katsnelson, A. Svane, O. Eriksson, Multiplet effects in the electronic structure of intermediate-valence compounds, Phys. Rev. B 79 (2009) 165104, doi:10.1103/PhysRevB.79.165104.

[30] M.S. Litsarev, I. DiMarco, P. Thunström, O. Eriksson, Correlated electronic structure and chemical bonding of ce pnictides and γ-Ce, Phys. Rev. B 86 (2012) 115116.

[31] O. Grns, I. Di Marco, P. Thunstrm, L. Nordstrm, O. Eriksson, T. Bjrkman, J. Wills, Charge self-consistent dynamical mean-field theory based on the full-potential linear muffin-tin orbital method: methodology and applications, Comput. Mater. Sci 55 (2012) 295–302, doi:10.1016/j.commatsci.2011.11.032. https://www.sciencedirect.com/science/article/pii/S092702561100646X.

[32] L.V.B. Diop, M.D. Kuz'min, Y. Skourski, K.P. Skokov, I.A. Radulov, O. Gutfleisch, Determination of the crystal field parameters in $SmFe_{11}Ti$, Phys. Rev. B 102 (2020) 064423.

[33] Y.G. Pastushenkov, K.P. Skokov, Y. Skourski, L. Lebedeva, T. Ivanova, A. Grushichev, K.H. Müller, Magnetocrystalline anisotropy and magnetic domain structure of $erfe_{11}ti$ and $hofe_{11}ti$ compounds, J. Magn. Magn. Mater. 300 (2006) e500.

[34] W. Sucksmith, J.E. Thompson, The magnetic anisotropy of cobalt, Proc. R. Soc. Lond. Ser. A. Math. Phys. Sci. 225 (1162) (1954) 362–375, doi:10.1098/rspa.1954.0209.

[35] M.B. Lyakhova, O.V. Zhdanova, Analysis of magnetization curves and magnetocrystalline anisotropy of uniaxial ferromagnets, Met. Sci. Heat Treat. 58 (2017) 587.

[36] A. Arrott, Criterion for ferromagnetism from observations of magnetic isotherms, Phys. Rev. 108 (1957) 1394.

[37] M.D. Kuz'min, Shape of temperature dependence of spontaneous magnetization of ferromagnets: quantitative analysis, Phys. Rev. Lett. 94 (2005) 107204.

[38] Q. Qi, Y.P. Li, J.M.D. Coey, Gas-phase interstitially modified intermetallics $r(fe_{11}ti)z_{1-\delta}$: II 3d magnetization of the compounds $y(fe_{11}ti)z_{1-\delta}$ (z=n, c), J. Phys.: Cond. Matt. 4 (1992) 8209.

[39] P. Wolfers, M. Bacmann, D. Fruchart, Single crystal neutron diffraction investigations of the crystal and magnetic structures of r2fe14b (r=y, nd, ho, er), J. Alloys Compd. 317–318 (2001) 39–43, doi:10.1016/S0925-8388(00)01353-0. The 13th International Conference on Solid Compounds of Transition Elements

[40] G. Asti, F. Bolzoni, Theory of first order magnetization processes: uniaxial anisotropy, J. Magn. Magn. Mater. 20 (1980) 29.

[41] F. Bolzoni, O. Moze, First order field induced magnetization transitions in single crystal $Nd_2Fe_{14}b$, J. Appl. Phys. 62 (1987) 615.

[42] D.Y. Karpenkov, K. Skokov, M. Lyakhova, I. Radulov, T. Faske, Y. Skourski, O. Gutfleisch, Intrinsic magnetic properties of hydrided and non-hydrided nd_5fe_{17} single crystals, J. Alloys Compd. 741 (2018) 1012–1020, doi:10.1016/j.jallcom.2018.01.239. https://www.sciencedirect.com/science/article/pii/S0925838818302469.

[43] L. Néel, Les lois de laimantation et de la subdivision en domaines élémentaires dun monocristal de fer, J. Phys. le Radium 5 (1944) 265.

[44] R. Birss, D.J. Martin, The magnetization process in hexagonal ferromagnetic and ferrimagnetic single crystals, J. Phys. C Solid State Phys. 8 (1975) 189.

[45] H. Kronmüller, H. Träuble, A. Seeger, O. Boser, Theorie der anfangssuszeptibilitt und der magnetisierungskurve von hexagonalen kobalt-einkristallen, Mater. Sci. Eng. 1 (1966) 91.

[46] K.P. Skokov, Y.G. Pastushenkov, S.V. Taskaev, V.V. Rodionova, Micromagnetic analysis of spin-reorientation transitions. the role of magnetic domain structure, Physica B 478 (2015) 12–16, doi:10.1016/j.physb.2015.08.044. https://www.sciencedirect.com/science/article/pii/S0921452615301940.

[47] G. Asti, F. Bolzoni, F. Leccabue, R. Panizzieri, L. Pareti, S. Rinaldi, High field first order transitions in $prco_{5\pm x}$: the role of the K_3 anisotropy constant, J. Magn. Magn. Mater. 15–18 (1980) 561–562, doi:10.1016/0304-8853(80)90664-2. https://www.sciencedirect.com/science/article/pii/0304885380906642.

[48] F. Bolzoni, M.F. Pirini, Competing anisotropies and first order magnetization processes, J. Appl. Phys. 68 (1990) 2315.

[49] M.D. Kuz'min, Y. Skourski, K.P. Skokov, K.-H. Müller, O. Gutfleisch, Determining anisotropy constants from a first-order magnetization process in Tb_2Fe_{17}, Phys. Rev. B 77 (2008) 132411, doi:10.1103/PhysRevB.77.132411.

[50] K.P. Skokov, Y.G. Pastushenkov, S.A. Nikitin, M. Fries, O. Gutfleisch, Rotational magnetocaloric effect in the $Er_2Fe_{14}b$ single crystal, IEEE Trans. Magn. 52 (2016) 25000304.

[51] S.A. Nikitin, I.S. Tereshina, V.N. Verbetskiĭ, A. Salamova, Magnetic anisotropy of $yfe_{11}ti$ and its hydrids, Phys. Sol. State 40 (1998) 258.

[52] C. Piquer, F. Grandjean, O. Isnard, V. Pop, G.J. Long, A magnetic and mössbauer spectral study of the spin reorientation in $NdFe_{11}Ti$ and $NdFe_{11}TiH$, J. Appl. Phys. 95 (11) (2004) 6308–6316, doi:10.1063/1.1736333.

[53] Y. Yang, X. Zhang, S. Ge, Q. Pan, L. Kong, H. Li, J. Yang, B. Zhang, Y. Ding, C. Ye, Magnetic and crystallographic properties of novel fe rich rare earth nitrides of the type $RTiFe_{11}N_{1\delta}$ (invited), J. Appl. Phys. 70 (10) (1991) 6001–6005, doi:10.1063/1.350074.

[54] A. Sakuma, Electronic structure and magnetism of $YFe_{11}Ti$, J. Appl. Phys. 73 (1993) 6922.

[55] L. Ke, D.A. Kukusta, D.D. Johnson, Origin of magnetic anisotropy in doped $\mathbf{ce_2co}_{17}$ alloys, Phys. Rev. B 94 (2016) 144429, doi:10.1103/PhysRevB.94.144429.

[56] A. Vishina, O. Eriksson, O.Y. Vekilova, A. Bergman, H.C. Herper, Ab-initio study of the electronic structure and magnetic properties of Ce_2Fe_{17}, J. Alloys Compd. 888 (2021) 161521, doi:10.1016/j.jallcom.2021.161521.

[57] T. Zhao, X.C. Kou, Z.D. Zhang, X.K. Sun, Y.C. Chuang, F.R. de Broer, Magnetic properties of $R(Fe,Mn)_{11}Ti$ compounds, J. Appl. Phys. 79 (1996) 6324.

[58] T. Miyaki, K. Terakura, Y. Harashima, H. Kino, S. Ishibashi, First-principles study of magnetocrystalline anisotropy and magnetization in $NdFe_{12}$, $NdFe_{11}Ti$, and $NdFe_{11}TiN$, J. Phys. Soc. Japan 83 (2014) 042702.

[59] J.M.D. Coey, Hard magnetic materials: a perspective, IEEE Trans. Magn. 47 (2011) 4671.

[60] Electrons at the fermi surface, M. Springford (Ed.), Cambridge University Press, Cambridge, England, 1980.

[61] G.H.O. Daalderop, P.J. Kelly, M.F.H. Schuurmans, First-principles calculation of the magnetocrystalline anisotropy energy of iron, cobalt, and nickel, Phys. Rev. B 41 (1990) 11919–11937, doi:10.1103/PhysRevB.41.11919.

[62] B.-P. Hu, H.-S. Li, J.M.D. Coey, J.P. Gavigan, Magnetization of a $DyFe_{11}Ti$ single crystal, Phys. Rev. B 41 (1990) 2221–2228, doi:10.1103/PhysRevB.41.2221.

[63] A. Alam, D.D. Johnson, Mixed valency and site-preference chemistry for cerium and its compounds: a predictive density-functional theory study, Phys. Rev. B 89 (2014) 235126, doi:10.1103/PhysRevB.89.235126.

[64] H.C. Herper, T. Ahmed, J.M. Wills, I. Di Marco, T. Björkman, D. Iuşan, A.V. Balatsky, O. Eriksson, Combining electronic structure and many-body theory with large databases: a method for predicting the nature of $4f$ states in Ce compounds, Phys. Rev. Materials 1 (2017) 033802, doi:10.1103/PhysRevMaterials.1.033802.

[65] H.C. Herper, O.Y. Vekilova, S.I. Simak, I.D. Marco, O. Eriksson, Localized versus itinerant character of 4f-states in cerium oxides, Journal of Physics: Condensed Matter 32 (21) (2020) 215502, doi:10.1088/1361-648x/ab6e92.